Sensitivity analysis of distributed acoustic sensing arrays

Eileen R. Martin, Biondo Biondi, Gabriel Fabien-Ouellet, and Robert G. Clapp

ABSTRACT

Distributed acoustic sensing (DAS) measures the average axial strain (strain rate) along a subset of a fiber optic cable, as opposed to the particle displacement (velocity) at a particular small point sensor. In shifting from measuring a vector field to a tensor field, DAS effectively increases the directional sensitivity of measurements of every type of seismic wave when compared to single-component geophones. This switch from vector to tensor quantities leads to a plausible explanation for sign-flips between orthogonal channels seen during some S-wave and surface-wave events in our recordings of earthquakes. We show this through theoretical analysis of planar Rayleigh, Love, P- and S-waves over both infinitesimally small and realistic gauge lengths. We extend the analysis of individual sensor detection of surface waves to inter-receiver cross-correlations of these detections showing even more directionally-dependent sensitivity trends than individual sensors.

INTRODUCTION

It is well known that DAS channels have more extreme sensitivity patterns to waves incident on the fiber at an angle than single-component geophones (Kuvshinov, 2016), but there are in fact more complex relationships at play, particularly as we pursue arrays with increasingly more unusual geometry. In many of our recordings of earthquakes at the Stanford Distributed Acoustic Sensing Array (SDASA-1), we noticed a recurring pattern, particularly after the arrival of S-waves: fibers that were parallel would extend at the same time fibers in the orthogonal direction would compress. Immediately following the P-wave arrivals, it was less clear whether this behavior was observed. Examples of this behavior can also be seen at the L-shaped DAS array at the Richmond Field Station, and the orthogonal grid lines in Fairbanks, AK. Previously, we hypothesized based on 2D tensor rotation math that this was to be expected for waves which propagate orthogonal to their direction of particle motion (Biondi et al., 2017). In this report, we aim to better understand how angle of incidence, wavenumber, and gauge length modify DAS recordings of plane waves, building on the work of (Kuvshinov, 2016).

Here, we work through the 3D math for sensitivity assuming infinitesimally small gauge length, which predicts the same trends: P-waves and Rayleigh waves recorded

on orthogonal channels are equal up to a factor of $\tan^2(\theta)$, where θ is the angle between one fiber and the wave propagation direction, while Love waves are equal up to a factor of -1. S-wave recordings are made up of two terms: one that orthogonal channels record up to a factor of $\tan^2(\theta)$, and the other which is recorded up to a factor of -1. The balance between these two terms is determined by the angle between the polarization direction and the horizontal surface that the two orthogonal fibers lay on, so that if the S-wave's particle motion direction is perfectly horizontal, it would show the same trend as a Love wave.

From the plane wave analysis with infinitesimally small gauge length, we calculate the response of a channel with finite gauge length responding to each type of plane wave coming from any angle to better understand earthquake and active source response. Essentially, the angular sensitivity response begins to develop blind angles (like frequency notches, but in space!), which increase in angular density as the wavenumber increases.

Once we understand the response of a single channel to a plane surface-wave, we analyze the response of a pair of sensors to that same plane wave. Naturally, the directional sensitivity is made even more extreme by combining both receiver sensitivity responses. For Rayleigh waves detected by colinear channels, this makes little difference since sources traveling in-line with the sensor pair are preferentially sensed.

But for Love waves detected by parallel non-colinear channels, this often leads to false apparent velocity increases even in the presence of an angularly uniform noise field. Previously we had used a simple model to express interferometry of parallel channels as a linear combination of Love wave Green's function estimates that would each yield the proper velocity (Martin and Biondi, 2017), but we had neglected to consider destructive interference in the signals could lead to false apparent velocities. Understanding these responses is the first step towards correcting for them and extracting true Love wave velocities, as well as learning to use channels at an arbitrary orientation with respect to each other.

PREDICTED EFFECT OF FIBER ORIENTATION ON RECORDED PLANE WAVES

In this section, we assume an infinitesimally small gauge length, and calculate the axial strain along a fiber in the direction $(\cos(\theta), \sin(\theta), 0)$ for any $\theta \in [0, 2\pi)$ as it reacts to multiple types of body and surface waves:

- Rayleigh waves propagating in the direction $(x, 0, 0)$ with particle motion in the x and z directions
- P-waves propagating in the direction $(x, 0, z)$ with particle motion in the same direction

- Love waves propagating in the direction $(x, 0, 0)$ with particle motion in the y direction
- S-waves propagating in the direction $(x, 0, z)$ with particle motion in any direction perpendicular to the direction of propagation (special cases: particle motion parallel to $x - z$ plane or $x - y$ plane)

Note that the orientation of the fiber can change freely enough that we simply change our coordinate system to line up the $x - z$ plane with the wave propagation direction. All results that follow can be easily transferred to strain-rate by taking a time derivative. For each type of wave, we calculate the expected response for:

1. a point-wise axial strain measurement of a horizontal straight fiber
2. the point-wise axial strain measurement of an orthogonal horizontal straight fiber
3. the average axial strain throughout one channel of a horizontal straight fiber

We make the simple assumption that DAS measurement is the average axial strain rate along one gauge length centered at (x, y, z), called $\bar{\sigma}(x, y, z, t)$, with all points weighted equally. Modifications of how the interrogator unit is implemented may change the data from theoretical ideals predicted here (Bona et al., 2017), but that information is typically not available to the user and may be considered a secondary effect.

As our starting point for understanding strain data, we have some strain tensor field observed in the (x, y, z) coordinate system:

$$\Sigma(x,y,z,t) = \begin{bmatrix} \frac{\partial u_x}{\partial x} & \frac{1}{2}\left(\frac{\partial u_x}{\partial y} + \frac{\partial u_y}{\partial x}\right) & \frac{1}{2}\left(\frac{\partial u_x}{\partial z} + \frac{\partial u_z}{\partial x}\right) \\ \frac{1}{2}\left(\frac{\partial u_y}{\partial x} + \frac{\partial u_x}{\partial y}\right) & \frac{\partial u_y}{\partial y} & \frac{1}{2}\left(\frac{\partial u_y}{\partial z} + \frac{\partial u_z}{\partial y}\right) \\ \frac{1}{2}\left(\frac{\partial u_z}{\partial x} + \frac{\partial u_x}{\partial z}\right) & \frac{1}{2}\left(\frac{\partial u_z}{\partial y} + \frac{\partial u_y}{\partial z}\right) & \frac{\partial u_z}{\partial z} \end{bmatrix}. \tag{1}$$

However, we are generally most interested in the axial strain as observed by some horizontal fiber at an angle θ from the x direction, so that is represented by the $(0, 0)$ entry of the strain tensor rotated into the coordinate system of the fiber (using shorthand that $\mathcal{S}_\theta = \sin(\theta)$ and $\mathcal{C}_\theta = \cos(\theta)$:

$$\Sigma_\theta(x,y,z,t) = \begin{bmatrix} \mathcal{C}_\theta & \mathcal{S}_\theta & 0 \\ -\mathcal{S}_\theta & \mathcal{C}_\theta & 0 \\ 0 & 0 & 1 \end{bmatrix} \Sigma(x,y,z,t) \begin{bmatrix} \mathcal{C}_\theta & -\mathcal{S}_\theta & 0 \\ \mathcal{S}_\theta & \mathcal{C}_\theta & 0 \\ 0 & 0 & 1 \end{bmatrix}. \tag{2}$$

So the $(0, 0)$ entry of this, representing the axial strain at the point (x, y, z) in the θ direction is

$$\sigma(x,y,z,t) = \mathcal{C}_\theta^2 \frac{\partial u_x}{\partial x} + \mathcal{C}_\theta \mathcal{S}_\theta \left(\frac{\partial u_x}{\partial y} + \frac{\partial u_y}{\partial x}\right) + \mathcal{S}_\theta^2 \frac{\partial u_y}{\partial y} \tag{3}$$

Rayleigh Waves

As in Pujol (2003), we consider a monochromatic Rayleigh plane wave propagating in the x direction at phase velocity c, frequency $\omega = kc$, and wavenumber k in a half space:

$$\mathbf{u}(x,y,z,t) = \left((Ae^{-\gamma_\alpha kz} + iB\gamma_\beta e^{-\gamma_\beta kz})e^{ik(ct-x)}, 0, (-iA\gamma_\alpha e^{-\gamma_\alpha kz} + Be^{-\gamma_\beta kz})e^{ik(ct-x)}\right), \tag{4}$$

where $\gamma_\delta = \sqrt{1 - \frac{c^2}{\delta}}$ for $\delta = \alpha$ and β. Here, α and β are the irrotational and solenoidal parts of the solution to the elastic wave equation, so $\mathbf{u}_\alpha + \mathbf{u}_\beta = \mathbf{u}$, $\nabla \times \mathbf{u}_\alpha = 0$ and $\nabla \cdot \mathbf{u}_\beta = 0$ Following Equation 3, we can calculate the axial strain at a point (x, y, z) on a horizontal fiber at an angle θ counter-clockwise from the propagation direction to be:

$$\sigma(x,y,z,t) = \cos^2(\theta)\frac{\partial u_x}{\partial x} = -ik\cos^2(\theta)(Ae^{-\gamma_\alpha kz} + iB\gamma_\beta e^{-\gamma_\beta kz})e^{ik(ct-x)} \tag{5}$$

so we can split this into a geometry-dependent amplitude factor, $-ik\cos^2(\theta)(Ae^{-\gamma_\alpha kz} + iB\gamma_\beta e^{-\gamma_\beta kz})e^{-ikx}$, multiplied by an oscillatory factor, e^{ikct}. That geometry-dependent amplitude factor is plotted for many angles in Figure 1. In the Stanford DAS Array, and multiple other surface DAS arrays in existance, a common trait is that the lines primarily follow two orthogonal directions, so let's investigate the relationship between the observation at an angle θ and $\theta + \frac{\pi}{2}$. Along this orthogonal line at the same location, we expect to measure:

$$\sigma^\perp(x,y,z,t) = \cos^2\left(\theta + \frac{\pi}{2}\right)\frac{\partial u_x}{\partial x} = \frac{\sin^2(\theta)}{\cos^2(\theta)}\sigma(x,y,z,t). \tag{6}$$

Thus, this rotation is only expected to lead to a $\tan^2(\theta)$ amplitude change, not a shift in the oscillatory part of the signal.

More realistically, we expect to measure the average axial strain along a segment of fiber of length g, the gauge length. This is expected to lead to notches in the FK spectrum. Thus, if we had a channel oriented at the angle θ spanning $(x - \frac{g}{2}\cos(\theta), y - \frac{g}{2}\sin(\theta), z)$ to $(x + \frac{g}{2}\cos(\theta), y + \frac{g}{2}\sin(\theta), z)$, it would measure:

$$\begin{aligned}
\bar{\sigma}(x,y,z,t) &= \int_{-g/2}^{g/2} \sigma(x + \nu\cos(\theta), y + \nu\sin(\theta), 0)d\nu \\
&= -ik\cos^2(\theta)(A + iB\gamma_\beta)e^{ikct}\int_{-g/2}^{g/2} e^{-ik(x+\nu\cos(\theta))}d\nu \\
&= -ik\cos^2(\theta)(A + iB\gamma_\beta)e^{ikct}e^{-ikx}\left[\frac{e^{-ik\nu\cos(\theta)}}{-ik\cos(\theta)}\right]_{\nu=-g/2}^{g/2} \\
&= \cos(\theta)(A + iB\gamma_\beta)e^{ikct}e^{-ikx}(e^{ik\frac{g}{2}\cos(\theta)} - e^{-ik\frac{g}{2}\cos(\theta)}) \\
&= 2i\cos(\theta)(A + iB\gamma_\beta)e^{ik(ct-x)}\sin(\frac{kg}{2}\cos(\theta)).
\end{aligned} \tag{7}$$

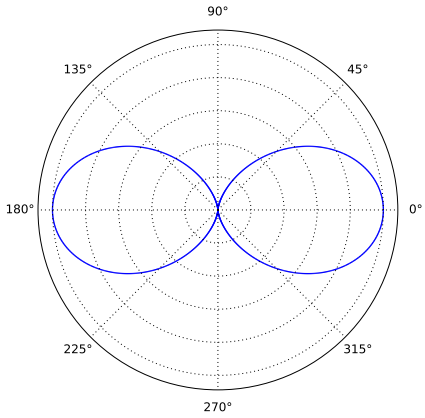

Figure 1: The radius of this polar plot represents the axial strain sensitivity along a horizontal fiber reacting to Rayleigh plane waves propagating at many angles θ. The amplitude of this sensitivity is proportional to wavenumber, k, but its shape is independent of wavenumber. [**ER**]

As a sanity check, this makes sense because it says all fiber channels centered on a given x coordinate (and any x coordinates offset by $2\pi/k$) will measure the same response as the plane wave rolls through, propagating in the x direction. The factor $\cos(\theta)\sin(kg\cos(\theta)/2)$ determines the sensitivity of a given channel to plane waves incident on the fiber at an angle θ, so we see that not only orientation, but also the wavenumber-gauge length relationship play an important role in the detected signal. Polar plots of this sensitity for various kg values are plotted in Figure 2. We see that this bears some similarity to the usual $\cos^2$ sensitivity, but with a more complex interaction leaving increasingly more frequency notches as k and/or g increase.

As seen in Figure 2, when k is small the sensitivity pattern's shape resembles that of the point-wise measurement. There are two ways to see that in fact the limit as $k \to 0$ the sensitivity converges to the point limit. We could define the 'shape' of the sensitivity to be the ratio in sensitivity between any two angles, θ_1 and θ_2, which for point-wise measurements is:

$$R(\theta_1, \theta_2) = \frac{\cos^2(\theta_1)\sin^2(\phi_1)}{\cos^2(\theta_2)\sin^2(\phi_2)} \tag{8}$$

Then the channel-wise measurement ratio, R_c is:

$$R_c(\theta_1, \theta_2, k) = \frac{\cos(\theta_1)\sin(\phi_1)\sin(0.5kg\cos(\theta_1)\sin(\phi_1))}{\cos(\theta_2)\sin(\phi_2)\sin(0.5kg\cos(\theta_2)\sin(\phi_2))} \tag{9}$$

and if we take the limit as $k \to 0$ using L'Hospital's rule:

$$\begin{aligned} R_c(\theta_1, \theta_2, 0) &= \frac{\cos(\theta_1)\sin(\phi_1)\cos(0.5 * 0 * g\cos(\theta_1)\sin(\phi_1))0.5g\cos(\theta_1)\sin(\phi_1)}{\cos(\theta_2)\sin(\phi_2)\cos(0.5 * 0 * g\cos(\theta_2)\sin(\phi_2))0.5g\cos(\theta_2)\sin(\phi_2)} \\ &= \frac{\cos^2(\theta_1)\sin^2(\phi_1)}{\cos^2(\theta_2)\sin^2(\phi_2)} \end{aligned} \tag{10}$$

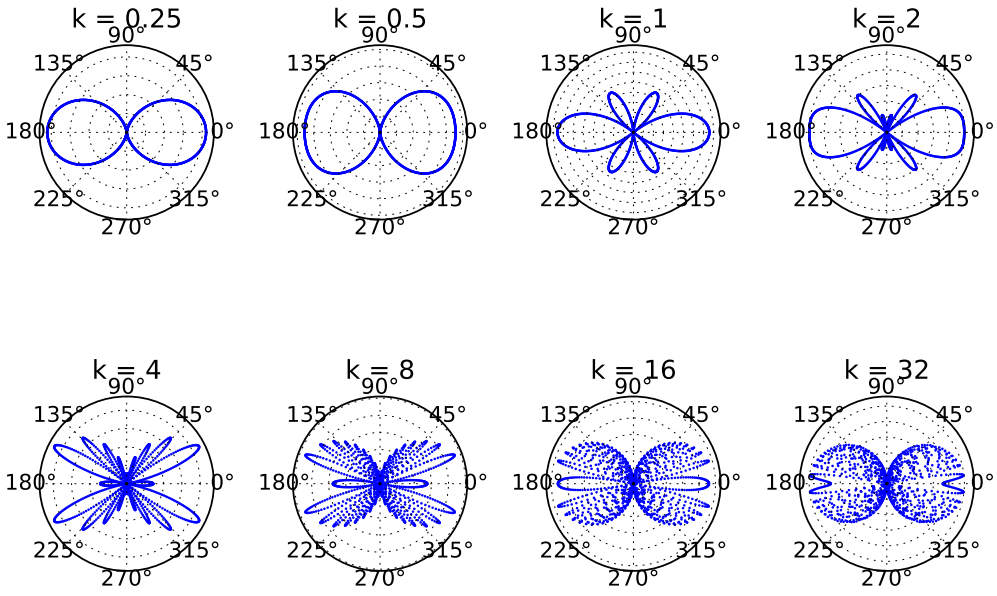

Figure 2: The radius of these polar plots represents the axial strain sensitivity along a horizontal fiber reacting to Rayleigh plane waves propagating at an angle θ relative to the fiber for multiple wavenumbers, k, assuming a gauge length $g = 8$ meters. Each plot is normalized so the peak sensitivity angle appears to be the same radius. [**ER**]

which is the same as the point-wise angular sensitivity ratio. More simply, we can look at the Taylor series expansion about $k = 0$ for the channel sensitivity then drop the small nonlinear higher order terms:

$$\cos(\theta)\sin(\frac{kg}{2}\cos(\theta)) \approx \cos(\theta)\left[\frac{kg}{2}\cos(\theta) + \frac{(kg)^3}{8}\cos^3(\theta) + \dots\right] \propto kg\cos^2(\theta) \quad (11)$$

so we see it is proportional to the point-wise measurement solution. This observation in fact holds true to the rest of the wave types as well, as verified in the appendix.

P-Waves

Similar to Rayleigh waves, P-waves have particle motion in the same direction as their propagation (but no orthogonal rolling motion). As in Pujol (2003)

$$\mathbf{u}(x,y,z,t) = \left(A\sin(\phi)e^{i\omega(t-(x\sin(\phi)-z\cos(\phi))/\alpha)}, 0, -A\cos(\phi)e^{i\omega(t-(x\sin(\phi)-z\cos(\phi))/\alpha)}\right) \quad (12)$$

is the equation for a monochromatic plane P-wave traveling at velocity α at frequency ω, where ϕ is the angle between the z-axis and the direction of propagation. Again, $u_y = 0$, so the axial strain at a given point on a horizontal fiber at an angle θ from the x-axis is:

$$\sigma(x,y,z,t) = -i\cos^2(\theta)\frac{\omega}{\alpha}A\sin^2(\phi)e^{i\omega(t-(x\sin(\phi)-z\cos(\phi))/\alpha)}. \quad (13)$$

The geometry-dependent amplitude factor depends on the orientation of the fiber with respect to the wave propagation direction, but not on the wavenumber, as seen in Figures 3a and 3b. If we were to also have a colocated orthogonal horizontal fiber, it would simultaneously be sensitive to

$$\sigma^{\perp}(x,y,z,t) = \cos^2(\theta+\frac{\pi}{2})\frac{\partial u_x}{\partial x} = \frac{sin^2(\theta)}{\cos^2(\theta)}\sigma(x,y,z,t), \quad (14)$$

and so like the Rayleigh wave, we expect orthogonal observations of P-waves to exhibit only an amplitude difference proportional to $\tan^2$ of the angle between the horizontal projection of the propagation direction and one of the fibers, but no phase shift assuming point measurements.

Again, assume we have a channel oriented at the angle θ spanning $(x-\frac{g}{2}\cos(\theta), y-$

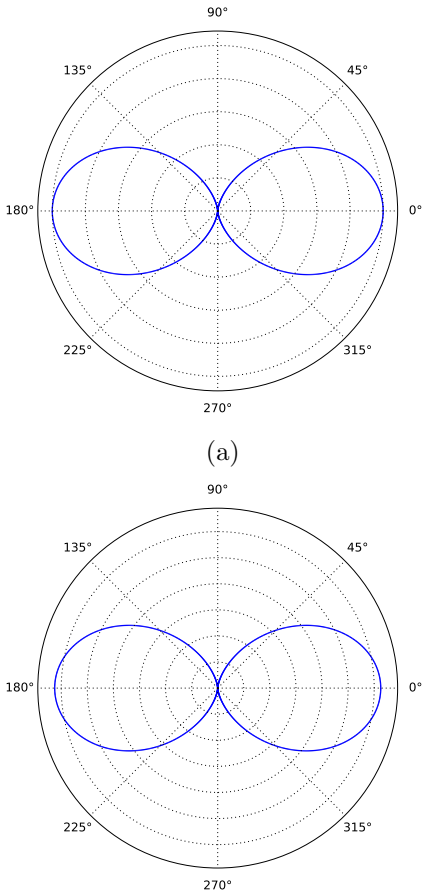

(a)

(b)

Figure 3: The radius of these polar plots represents the axial strain sensitivity along a horizontal fiber oriented at that angle θ from the horizontal propagation direction of a P-wave which is also propagating at an angle ϕ from vertical. The ϕ values plotted here are (top) $\pi/2$ and (bottom) $\pi/4$. The shape of these sensitivities (the ratio between the radii of any two angles) is constant with respect to both parameters. [**ER**]

$\frac{g}{2}\sin(\theta), z)$ to $(x+\frac{g}{2}\cos(\theta), y+\frac{g}{2}\sin(\theta), z)$, so it would measure:

$$\begin{aligned}
\bar{\sigma}(x,y,z,t) &= \int_{-g/2}^{g/2} -i\cos^2(\theta)\frac{\omega}{\alpha}A\sin^2(\phi)e^{i\omega(t-((x+\nu\cos(\theta))\sin(\phi)-z\cos(\phi))/\alpha)}d\nu \\
&= -i\cos^2(\theta)\frac{\omega}{\alpha}A\sin^2(\phi)e^{i\omega(t+z\cos(\phi)/\alpha)}e^{-i\omega x\sin(\phi)/\alpha}\int_{-g/2}^{g/2} e^{-i\omega\nu\cos(\theta)\sin(\phi)/\alpha}d\nu \\
&= -i\cos^2(\theta)\frac{\omega}{\alpha}A\sin^2(\phi)e^{i\omega(t+z\cos(\phi)/\alpha)}e^{-i\omega x\sin(\phi)/\alpha}\left[\frac{e^{-i\omega\nu\cos(\theta)\sin(\phi)/\alpha}}{-i\omega\cos(\theta)\sin(\phi)/\alpha}\right]_{-g/2}^{g/2} \\
&= \cos(\theta)A\sin(\phi)e^{i\omega(t+z\cos(\phi)/\alpha)}e^{-i\omega x\sin(\phi)/\alpha}(e^{-i\omega g\cos(\theta)\sin(\phi)/(2\alpha)} - e^{i\omega g\cos(\theta)\sin(\phi)/(2\alpha)}) \\
&= 2iA\cos(\theta)\sin(\phi)e^{i\omega(t-(x\sin(\phi)-z\cos(\phi))/\alpha)}\sin(\omega g\cos(\theta)\sin(\phi)/(2\alpha)). \qquad (15)
\end{aligned}$$

This easily splits into a time-dependent oscillatory part $e^{i\omega t}$, a geometry-dependent spatial oscillatory part (dependent on apparent wavenumber where the true wavenumber $k=\omega/\alpha$): $e^{-ik(x\sin(\phi)-z\cos(\phi))}$, and a geometry-dependent amplitude factor proportional to $\cos(\theta)\sin(\phi)\sin(\omega g\cos(\theta)\sin(\phi)/(2\alpha))$. We can simplify the amplitude factor a little to be $\cos(\theta)\sin(\phi)\sin(kg\cos(\theta)\sin(\phi)/2)$ where $k=\omega/\alpha$, so like in the Rayleigh wave observations, our amplitude depends on the product of the wavenumber and gauge length as well as the orientation between the fiber and the propagation direction of the wave.

A quick check that this is reasonable: if $\phi=0$ the wave is vertically propagating, and a horizontal fiber should be insensitive to it, which we verify because the $\sin(\phi)$ factor in the amplitude is 0. Assuming $\phi=\pi/2$ (the special case of horizontally propagating P-waves), plots of the amplitude factor for various kg values are shown in Figures 4a and 4b. Again, we mostly see a pattern that is like the frequently quoted $\cos^2$ sensitivity trend, but as the wavenumber and/or gauge length increase, the fiber has increasingly more blind angles. Of course, real waves are composed of a range of frequencies, so even if part of the array misses a source at one frequency, it may still detect that source at other frequencies with the same gauge length.

Love Waves

Say that we have a half-space with a layer in the top H meters with group velocity β_1 and β_2 for the half-space underneath. In this scenario, a Love wave can propagate horizontally at phase velocity c in the x direction following the displacement equation:

$$\mathbf{u}(x,y,z,t) = \big(0, (Ae^{-i\eta_1 kz} + Be^{i\eta_1 kz})e^{ik(ct-x)}, 0\big) \qquad (16)$$

in the top layer ($z<H$) and

$$\mathbf{u}(x,y,z,t) = \big(0, Ce^{-\eta_2 kz+ik(ct-x)}, 0\big) \qquad (17)$$

in the bottom half. Note that $\eta_i = \sqrt{(c/\beta_i)^2-1}$. Here, we assume for simplicity that the horizontal DAS array is contained within the top layer. Following a similar

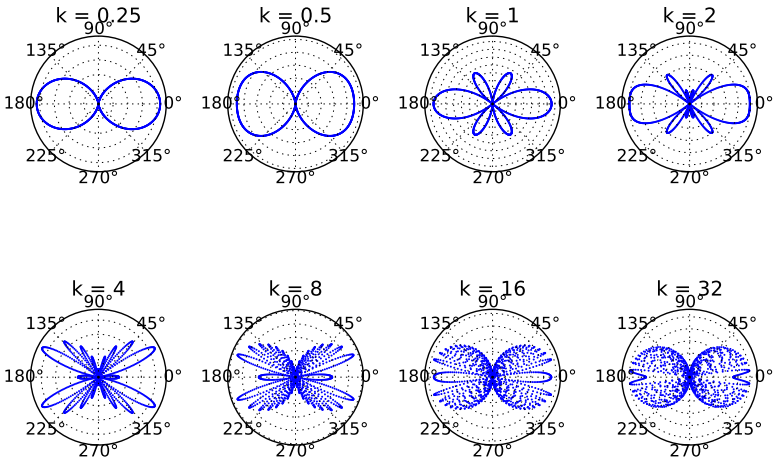

(a)

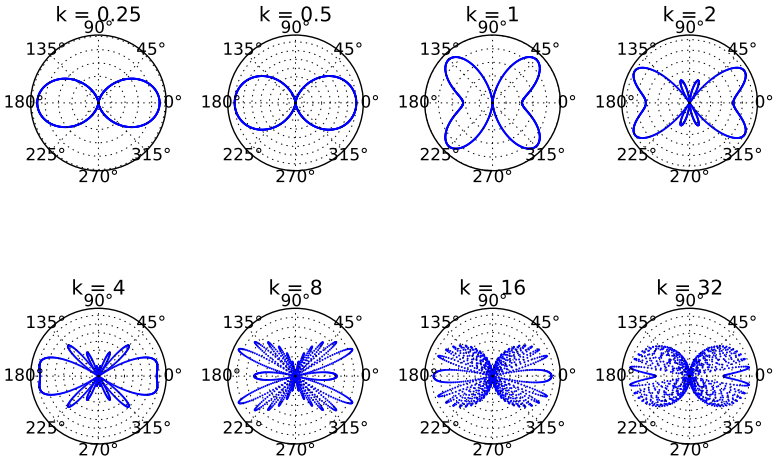

(b)

Figure 4: For a channel of gauge length $g = 8$ meters, the radius of these polar plots represents the axial strain sensitivity along a horizontal fiber oriented at that angle θ from the horizontal propagation direction of a P-wave which is also propagating at an angle ϕ from vertical. The ϕ values plotted here are (top) $\pi/2$ and (bottom) $\pi/4$. Unlike the case where only point-wise sensitivity is measured, the angular sensitivites varies significantly with angle. [**ER**]

procedure with the equation for the lower half could reveal Love wave response for a deeper horizontal buried array (perhaps a deviated well with fiber, or fiber installed in slim holes beneath the complexities of the near surface layer).

Following the same steps as above, we are interested in the strain rate of a fiber at a point oriented at an angle θ from the x-axis. In this case:

$$\begin{aligned}\sigma(x,y,z,t) &= \cos(\theta)\sin(\theta)\frac{\partial u_y}{\partial x} \\ &= -ik\cos(\theta)\sin(\theta)(Ae^{-i\eta_1 kz} + Be^{i\eta_1 kz})e^{ik(ct-x)}. \end{aligned} \tag{18}$$

We see the angular-dependent amplitude factor plotted in Figure 5, showing a four-lobe structure. This behaves quite differently than the two-lobe sensitivity of Rayleigh and P-waves.

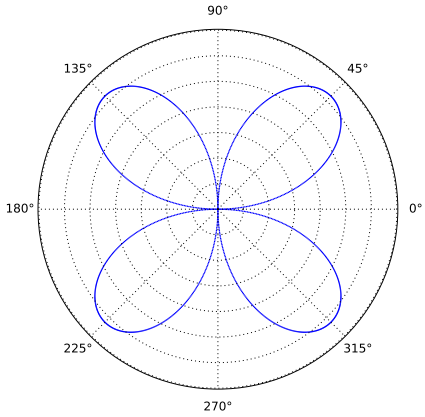

Figure 5: The radius of this polar plot represents the axial strain sensitivity along a horizontal fiber oriented at that angle θ from the horizontal propagation direction of a Love wave. Angular sensitivity is independent of wavenumber for a point measurement. [**ER**]

As before, we might wonder how Love waves appear on corners of arrays made of orthogonal lines. At the same point, an orthogonal fiber's axial strain would be:

$$\sigma^{\perp}(x,y,z,t) = \cos(\theta+\frac{\pi}{2})\sin(\theta+\frac{\pi}{2})\frac{\partial u_y}{\partial x} = -\sin(\theta)\cos(\theta)\frac{\partial u_y}{\partial x} = -\sigma(x,y,z,t), \tag{19}$$

suggesting that no matter what angle the plane wave is traveling, the orthogonal fibers will always record -1 times each other.

If we had a fiber channel of gauge length g oriented at the angle θ from the x-axis (direction of propagation) spanning $(x-\frac{g}{2}\cos(\theta), y-\frac{g}{2}\sin(\theta), z)$ to $(x+\frac{g}{2}\cos(\theta), y+$

$\frac{g}{2}\sin(\theta), z)$, that channel would actually measure:

$$\begin{aligned}
\bar{\sigma}(x,y,z,t) &= \int_{-g/2}^{g/2} -ik\cos(\theta)\sin(\theta)(Ae^{-i\eta_1 kz} + Be^{i\eta_1 kz})e^{ik(ct-(x+\nu\cos(\theta)))}d\nu \\
&= -ik\cos(\theta)\sin(\theta)(Ae^{-i\eta_1 kz} + Be^{i\eta_1 kz})e^{ik(ct-x)}\int_{-g/2}^{g/2} e^{-ik\nu\cos(\theta)}d\nu \\
&= -ik\cos(\theta)\sin(\theta)(Ae^{-i\eta_1 kz} + Be^{i\eta_1 kz})e^{ik(ct-x)}\left[\frac{e^{-ik\nu\cos(\theta)}}{-ik\cos(\theta)}\right]_{-g/2}^{g/2} \\
&= \sin(\theta)(Ae^{-i\eta_1 kz} + Be^{i\eta_1 kz})e^{ik(ct-x)}\left[e^{-ik\frac{g}{2}\cos(\theta)} - e^{ik\frac{g}{2}\cos(\theta)}\right] \\
&= 2i\sin(\theta)(Ae^{-i\eta_1 kz} + Be^{i\eta_1 kz})e^{ik(ct-x)}\sin(-\frac{kg}{2}\cos(\theta)) \qquad (20)
\end{aligned}$$

which again simplifies into a geometry- and wavenumber-dependent oscillatory part $(Ae^{-i\eta_1 kz} + Be^{i\eta_1 kz})e^{-ikx}$, a time-dependent oscillatory part e^{ikct}, and a geometry- and wavenumber-dependent amplitude part proportional to $\sin(\theta)\sin(-\frac{kg}{2}\cos(\theta)$. As seen in Figure 6, we get more frequency notches as kg increases, but note that for Love waves, the sensitivity frequency notches are imprinted over a four-lobe pattern similar to the single-point $\cos(\theta)\sin(\theta)$ sensitivity. These fiber channels are not sensitive at all to Love waves traveling in-line or orthogonal to the fiber, but rather are sensitive to waves travelling at angles. This leads to data that are very counter-intuitive for people used to particle velocity measurements, as a horizontal component of a 3C geophone would be maximally sensitive to Love waves propagating orthogonally to that component.

S-Waves

Here, we follow Pujol (2003) in the simple model that if we have an S-wave propagating in the $x-z$ plane at an angle ϕ from the vertical axis, then the SH and SV motions can be described in simple cases by:

$$\mathbf{u}(x,y,z,t) = e^{i\omega(t-(x\sin(\phi)-z\cos(\phi))/\beta)}\left(B\cos(\phi), C, B\sin(\phi)\right) \qquad (21)$$

where β is the propagation velocity. In this case the axial strain at a point on a horizontal fiber oriented at an angle θ from the x-axis is:

$$\begin{aligned}
\sigma(x,y,z,t) &= \cos^2(\theta)\frac{\partial u_x}{\partial x} + \cos(\theta)\sin(\theta)\frac{\partial u_y}{\partial x} \\
&= \cos^2(\theta)B\cos(\phi)(-i\omega\sin(\phi)/\beta)e^{i\omega(t-(x\sin(\phi)-z\cos(\phi))/\beta)} \\
&\quad + \cos(\theta)\sin(\theta)C(-i\omega\sin(\phi)/\beta)e^{i\omega(t-(x\sin(\phi)-z\cos(\phi))/\beta)} \\
&= \frac{-i\omega\sin(\phi)}{\beta}e^{i\omega(t-(x\sin(\phi)-z\cos(\phi))/\beta)}\cos(\theta)(B\cos(\theta)\cos(\phi) + C\sin(\theta)) \qquad (22)
\end{aligned}$$

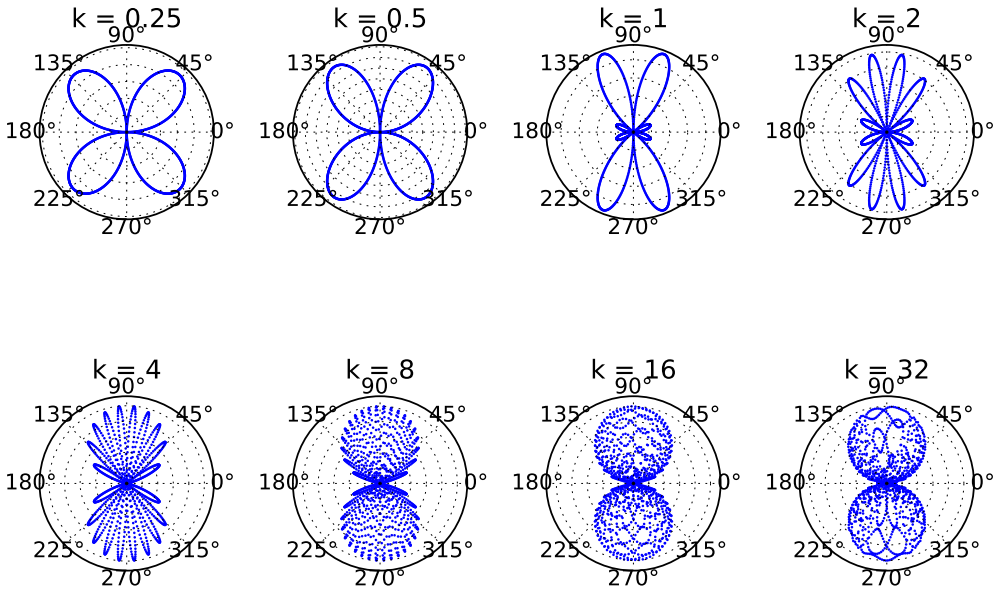

Figure 6: The radius of these polar plots represents the axial strain sensitivity of a channel along a horizontal fiber oriented at that angle θ from the horizontal propagation direction of a Love wave. We assume a gauge length of $g = 8$ meters, and show sensitivity for several wavenumbers, k, to emphasize that angular sensitivity is highly dependent on wavenumber, changing from a 4-lobe to almost being a 2-lobe structure (actually made up of many narrow lobes). [**ER**]

The factor in the point-wise axial strain sensitivity dependent on propagation angles can be seen in Figures 7a and 7b. The general trend is that we have a four-lobe structure, but the pair (and the angle of emphasis) of lobes that is larger depends on ϕ but is independent of k.

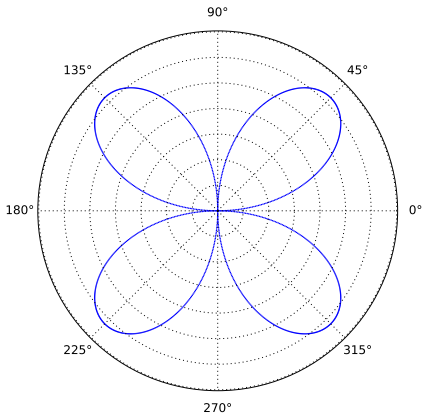

(a)

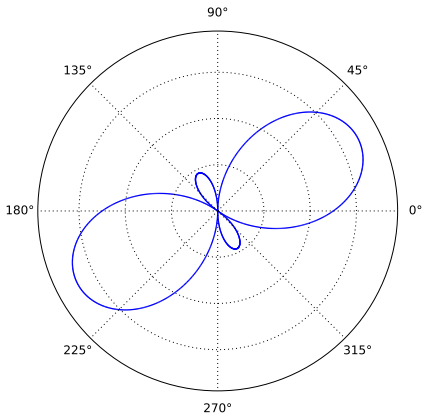

(b)

Figure 7: The radius of these polar plots represents the axial strain sensitivity along a horizontal fiber oriented at that angle θ from the horizontal propagation direction of an S-wave which is also propagating at an angle ϕ from vertical. The ϕ values plotted here are (top) $\pi/2$ and (bottom) $\pi/4$. The shape of the sensitivity is significantly affected by how much energy is propagating vertically, but is independent of wavenumber k. [**ER**]

Then if we wish to calculate the response of an orthogonal horizontal fiber at the

same point, it would be:

$$\begin{aligned}\sigma^{\perp}(x,y,z,t) &= \frac{-i\omega\sin(\phi)}{\beta}e^{i\omega(t-(x\sin(\phi)-z\cos(\phi))/\beta)}\cos(\theta+\pi/2)(B\cos(\theta+\pi/2)\cos(\phi)\\ &\quad +C\sin(\theta+\pi/2))\\ &= \frac{-i\omega\sin(\phi)}{\beta}e^{i\omega(t-(x\sin(\phi)-z\cos(\phi))/\beta)}\sin(\theta)(B\sin(\theta)\cos(\phi)-C\cos(\theta))\end{aligned} \tag{23}$$

Looking at just the last factors of that expression, we see that one term, $B\cos^2(\theta)\cos(\phi)$ changes to $B\sin^2(\theta)\cos(\phi)$, so it follows the previous trend in P and Rayleigh waves of a $\tan^2$ amplitude factor between orthogonal lines. The other term, $C\cos(\theta)\sin(\theta)$ becomes $-C\cos(\theta)\sin(\theta)$, so the orthogonal lines have a sign flip between their observations of this term, much like the Love waves.

In fact, this makes sense when we consider that when $\phi = \pi/2$ (the wave is travelling horizontally), and $\cos(\theta) = 0$, so it simplifies to see the same trend as Love waves. However, a shear wave has more degrees of freedom and as such contains a mix of behaviors.

Consider a horizontal fiber channel of gauge length g centered at (x, y, z) oriented at an angle θ from the x-axis, so it spans $(x-\frac{g}{2}\cos(\theta), y-\frac{g}{2}\sin(\theta), z)$ to $(x+\frac{g}{2}\cos(\theta), y+\frac{g}{2}\sin(\theta), z)$, that channel would actually measure:

$$\begin{aligned}\bar{\sigma}(x,y,z,t) &= \int_{-g/2}^{g/2}\frac{-i\omega\sin(\phi)}{\beta}e^{i\omega(t-((x+\nu\cos(\theta))\sin(\phi)-z\cos(\phi))/\beta)}\cos(\theta)\ldots\\ &\quad \times(B\cos(\theta)\cos(\phi)+C\sin(\theta))d\nu\\ &= -\frac{i\omega\sin(\phi)}{\beta}e^{i\omega(t-(x\sin(\phi)-z\cos(\phi))/\beta)}\cos(\theta)(B\cos(\theta)\cos(\phi)+C\sin(\theta))\ldots\\ &\quad \times\int_{-g/2}^{g/2}e^{-i\omega\nu\cos(\theta)\sin(\phi)/\beta}d\nu\\ &= e^{i\omega(t-(x\sin(\phi)-z\cos(\phi))/\beta)}(B\cos(\theta)\cos(\phi)+C\sin(\theta))\left[e^{-i\omega\nu\cos(\theta)\sin(\phi)/\beta}\right]_{-g/2}^{g/2}\\ &= 2ie^{i\omega(t-(x\sin(\phi)-z\cos(\phi))/\beta)}(B\cos(\theta)\cos(\phi)+C\sin(\theta))\sin\left(-\frac{\omega g\cos(\theta)\sin(\phi)}{2\beta}\right).\end{aligned}$$

Using the fact that $\omega/\beta = k$ our wavenumber, this simplifies to

$$\bar{\sigma}(x,y,z,t) = 2ie^{i\omega(t-(x\sin(\phi)-z\cos(\phi))/\beta)}(B\cos(\theta)\cos(\phi)+C\sin(\theta))\sin\left(\frac{-kg}{2}\cos(\theta)\sin(\phi)\right) \tag{24}$$

This easily factors into a temporal oscillatory part $e^{i\omega t}$, a geometry-dependent oscillatory part $e^{-i\omega(x\sin(\phi)-z\cos(\phi))/\beta}$, and a geometry-dependent amplitude factor proportional to $(B\cos(\theta)\cos(\phi)+C\sin(\theta))\sin(-kg\cos(\theta)\sin(\phi)/2)$.

When $\phi = 0$, the S-wave is traveling vertically. We expect zero sensitivity to both the SH and SV wave motions, which is what we get from that geometry-dependent

amplitude factor. Assume $\phi = \pi/2$, so it is an S-wave traveling horizontally. Then the sensitivity to plane waves coming in from the angle θ is seen in Figures 8a and 8b assuming $B = C = 1$. Again, the sensitivity gets more notches as kg grows, and in this case, the sensitivity shape starts out with the four-lobed shape similar to Love waves. One might wonder how getting further from the horizontal propagation direction affects this angular response, so the response for $\phi = \pi/4$ is plotted assuming $B = C = 1$ for a variety of kg values. Note that as k increases, the sensitivity approaches a two-lobe shape but is rotated depending on ϕ.

IMPLICATIONS FOR SURFACE WAVE CROSS-CORRELATIONS

During ambient noise interferometry, we are often extracting surface waves responding to virtual sources. These surface waves we extract can be used to infer near-surface features. Thus, we focus on the sensitivity of the cross-correlation of two receivers both detecting the same plane-wave source. The same sensitivity analysis could be repeated for body waves, although it is rare that researchers are able to extract body waves from ambient noise.

Rayleigh waves

First, let's look at how sensitive the cross-correlation of two colinear channels oriented at an angle θ form the x-axis are to planar Rayleigh waves propagating along the x-direction. Let's say the first channel spans $(-\frac{d}{2}\cos(\theta) - \frac{g}{2}\cos(\theta), -\frac{d}{2}\sin(\theta) - \frac{g}{2}\sin(\theta), 0)$ to $(-\frac{d}{2}\cos(\theta) + \frac{g}{2}\cos(\theta), -\frac{d}{2}\sin(\theta) + \frac{g}{2}\sin(\theta), 0)$, and the second channel spans $(\frac{d}{2}\cos(\theta) - \frac{g}{2}\cos(\theta), \frac{d}{2}\sin(\theta) - \frac{g}{2}\sin(\theta), 0)$ to $(\frac{d}{2}\cos(\theta) + \frac{g}{2}\cos(\theta), \frac{d}{2}\sin(\theta) + \frac{g}{2}\sin(\theta), 0)$. Following Equation 7, signals recorded by each of those channels are:

$$\begin{aligned}
\bar{\sigma}(-\frac{d}{2}\cos(\theta), -\frac{d}{2}\sin(\theta), 0, t) &= 2i\cos(\theta)(A + iB\gamma_\beta)e^{ik(ct+\frac{d}{2}\cos(\theta))}\sin(\frac{kg}{2}\cos(\theta)) \\
\bar{\sigma}(\frac{d}{2}\cos(\theta), \frac{d}{2}\sin(\theta), 0, t) &= 2i\cos(\theta)(A + iB\gamma_\beta)e^{ik(ct-\frac{d}{2}\cos(\theta))}\sin(\frac{kg}{2}\cos(\theta))
\end{aligned} \tag{25}$$

Thus their cross-correlation would be:

$$\begin{aligned}
C(\tau) &= \int_{-\infty}^{\infty} \bar{\sigma}(-\frac{d}{2}\cos(\theta), -\frac{d}{2}\sin(\theta), 0, t)\bar{\sigma}^*(\frac{d}{2}\cos(\theta), \frac{d}{2}\sin(\theta), 0, t+\tau)dt \\
&= \int_{-\infty}^{\infty} 4\cos^2(\theta)(A^2 - B^2\gamma_\beta^2)e^{ik(-c\tau+d\cos(\theta))}\sin^2(\frac{kg}{2}\cos(\theta))dt \\
&\approx 4\cos^2(\theta)(A^2 - B^2\gamma_\beta^2)e^{ik(-c\tau+d\cos(\theta))}\sin^2(\frac{kg}{2}\cos(\theta))
\end{aligned} \tag{26}$$

That last approximation is because that integral does not actually converge, but the terms have no dependence on t. Note that an integrable wavelet could be used to

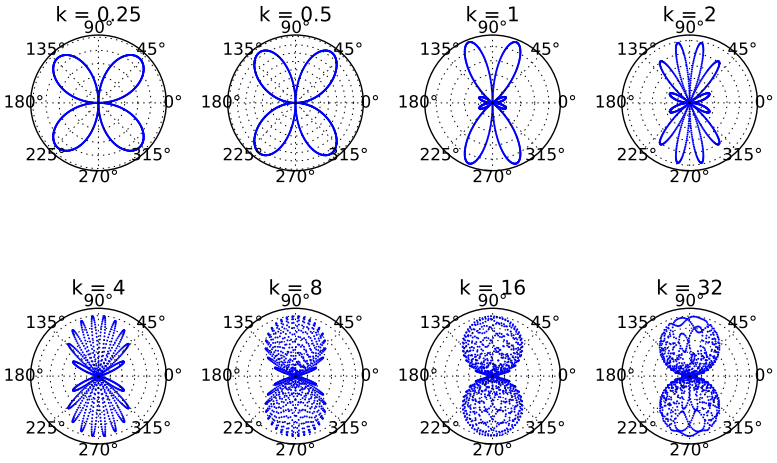

(a)

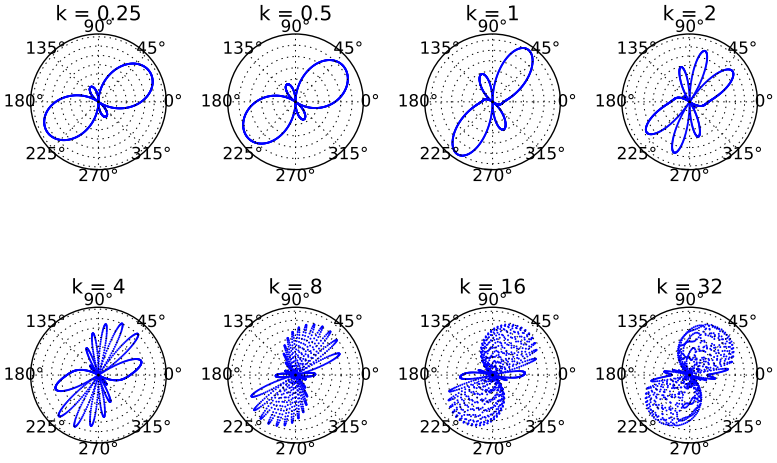

(b)

Figure 8: The radius of these polar plots represents the axial strain sensitivity of a channel along a horizontal fiber oriented at that angle θ from the horizontal propagation direction of an S-wave which is also propagating at an angle ϕ from vertical. The ϕ values plotted here are (top) $\pi/2$, which represents horizontally propagating S-waves, and (bottom) $\pi/4$. Note that the relative angular sensitivity to horizontally propagating S-waves is the same as Love waves. We assume a gauge length $g = 8$ meters. We see that the shape of the sensitivity is significantly affected by how much energy is propagating vertically. For both ϕ values, the sensitivities approach a 2-lobe-like shape, but when the S-wave is coming in at $\phi = \pi/4$, the lobes are rotated. [**ER**]

overcome this obstacle, for instance, convolution with a Gaussian around a particular start time, and the same angularly-dependent term would factor out. The term above does describe the geometric dependence of the cross-correlation on propagation direction and the distance between fiber channels. It has a temporal oscillatory factor, $e^{-ikc\tau}$, a spatial oscillatory term proportional to the apparent wavenumber times the distance between channels $e^{kd\cos(\theta)}$, and a spatial factor proportional to $\cos^2(\theta)\sin^2(kg\cos(\theta)/2)$, plotted in Figure 9

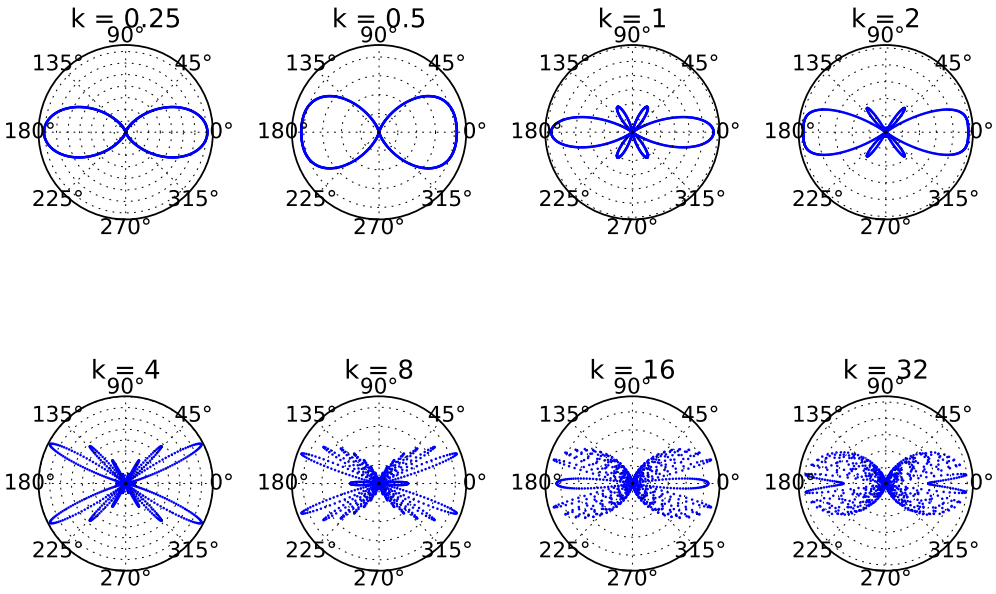

Figure 9: Assuming a set gauge length $g = 8$ meters, we plot the geometry-dependent amplitude factor as the radius at each angle θ, where that marks the angle between two parallel fiber channels and the propagation direction of a Rayleigh wave. Notice that as the wavenumber k increases, the sensitivity pattern moves away from a two-lobe pattern, then fills back in the two-lobe pattern. Thus at low and high wavenumbers, the cross-correlation emphasizes waves traveling straight from one channel to the other. [**ER**]

Love waves

Now let's look at the angular sensitivity of the cross-correlation of two parallel channels distance d apart with start and end points directly across from each other (as in Figure 10). One channel runs from $(\frac{d}{2}\sin(\theta) - \frac{g}{2}\cos(\theta), -\frac{d}{2}\cos(\theta) - \frac{g}{2}\sin(\theta), 0)$ to $(\frac{d}{2}\sin(\theta) + \frac{g}{2}\cos(\theta), -\frac{d}{2}\cos(\theta) + \frac{g}{2}\sin(\theta), 0)$, and the other runs from $(-\frac{d}{2}\sin(\theta) - \frac{g}{2}\cos(\theta), \frac{d}{2}\cos(\theta) - \frac{g}{2}\sin(\theta), 0)$ to $(-\frac{d}{2}\sin(\theta) + \frac{g}{2}\cos(\theta), \frac{d}{2}\cos(\theta) + \frac{g}{2}\sin(\theta), 0)$.

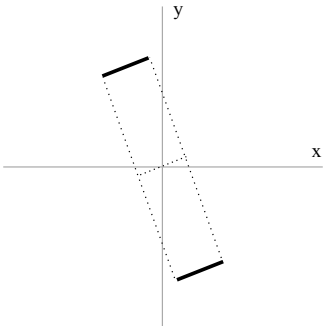

Figure 10: The dark lines represent two channels directly across from each other to be cross-correlated as they react to Love plane waves. [**NR**]

Following Equation 20, signals recorded by each of those channels are:

$$\begin{aligned}
\bar{\sigma}(\frac{d}{2}\sin(\theta), -\frac{d}{2}\cos(\theta), 0, t) &= 2i\sin(\theta)(A+B)e^{ik(ct-\frac{d}{2}\sin(\theta))}\sin(\frac{-kg}{2}\cos(\theta)) \\
\bar{\sigma}(-\frac{d}{2}\sin(\theta), \frac{d}{2}\cos(\theta), 0, t) &= 2i\sin(\theta)(A+B)e^{ik(ct+\frac{d}{2}\sin(\theta))}\sin(\frac{-kg}{2}\cos(\theta))
\end{aligned} \tag{27}$$

It follows that their cross-correlation would be:

$$\begin{aligned}
C_\tau &= \int_{-\infty}^{\infty} \bar{\sigma}(\frac{d}{2}\sin(\theta), -\frac{d}{2}\cos(\theta), 0, t)\bar{\sigma}^*(-\frac{d}{2}\sin(\theta), \frac{d}{2}\cos(\theta), 0, t) \\
&= \int_{-\infty}^{\infty} 4\sin^2(\theta)(A+B)^2 e^{-ik(c\tau+d\sin(\theta))}\sin^2(\frac{-kg}{2}\cos(\theta))dt \\
&\approx 4\sin^2(\theta)(A+B)^2 e^{-ik(c\tau+d\sin(\theta))}\sin^2(\frac{-kg}{2}\cos(\theta))
\end{aligned} \tag{28}$$

where again, we use the approximate symbol to indicate that the monochromatic wavelet is not integrable. This factors into an oscillatory time part $e^{ikc\tau}$, an oscillatory spatial part dependent on the apparent wavenumber and distance between channels $e^{-idk\sin(\theta)}$, and a geometry-dependent amplitude factor proportional to $\sin^2(\theta)\sin^2(\frac{-kg}{2}\cos(\theta))$.

However, the geometry-dependent amplitude factor, plotted in Figure 11 for many k values, starts at small wavenumbers (low frequencies) looking like the point measurements of Figure 5. At higher, more realistic wavenumbers, it approaches a two-lobe shape which is primarily sensitive to Love waves mostly traveling in-line with the radial direction between the two channels. However, if one is dealing with very low frequency/wavenumber signals, one absolutely must be aware that the four-lobe sensitivity pattern could lead to false apparent velocities in the interferometry of signals coming from all directions (as is assumed in ambient noise interferometry with a homogeneous angular distribution of far-field sources) which must be corrected for.

Additionally, even at higher wavenumbers, the zero-phase signal will never truly be picked up, so careful analysis of whether a Green's function can actually be extracted should be performed in the future.

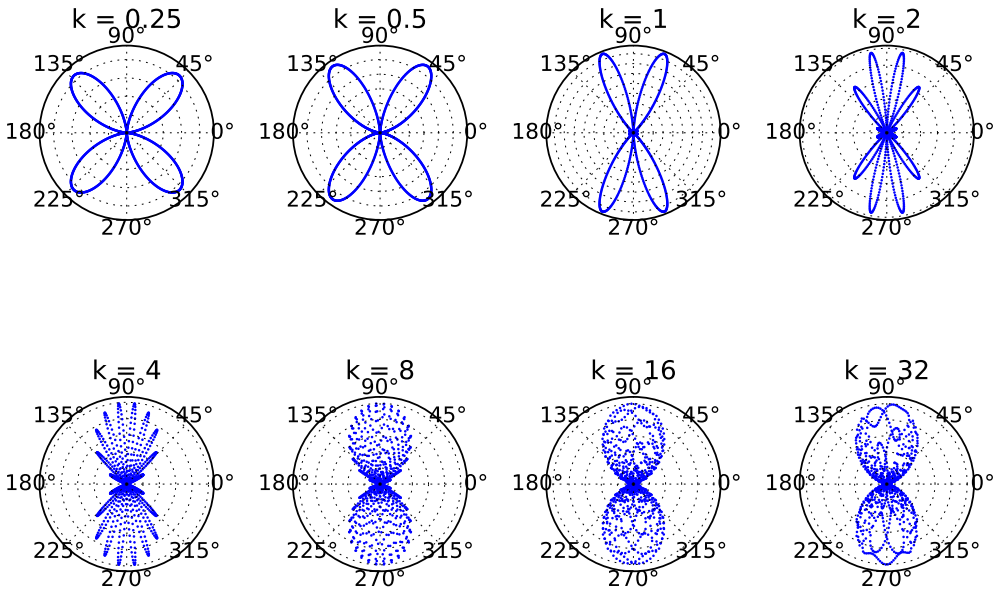

Figure 11: Assuming a set gauge length $g = 8$ meters, we plot the geometry-dependent amplitude factor as the radius at each angle, θ, where θ is the angle between two parallel fiber channels and the propagation direction of a Love wave. Notice that as the wavenumber k increases, the sensitivity pattern moves from a four-lobe pattern to a pattern with more lobes, then towards a two-lobe pattern which emphasizes waves traveling straight from one channel to the other. [**ER**]

PRACTICAL IMPLICATIONS OF SENSITIVITY

How should you choose your gauge length? All figures in this report have been generated assuming an 8 meter gauge length, and typical gauge length settings in seismic imaging/monitoring are 8-20 meters. However, you can use the same equations and generate sensitivity plots for a set k with many g values, with an increasing g having the same effect as an increasing k. Figures 6, 8a, 8b and 11 suggest that we would not want to use a very small g if we care about detecting S- and Love waves. This is particularly the case for ambient noise Love wave interferometry because the sensitivity at small kg is primarily to sources off at angles leading to false apparently high velocities. For a given k we can correct for these biases, but since the angular sensitivity peaks rotate as k increases for a set g, as seen in Figure 11, we would

need to correct for these biases independently for different wavelengths. This further suggests that for small kg the DAS interferometry results may include false dispersion trends. Thus, by using a g that is large enough for all expected k, we do not need to worry as much about these issues for Love wave interferometry. Rayleigh wave interferometry has much less of this issue at any kg.

In fact, for typical seismic wavelengths and gauge length settings, we tend to be on the low end of k values shown in this report. For instance, at the high end of seismic wavenumbers, a wavelength of 10 meters means a wavenumber $k \approx 0.63$, too low to see many of the unusual lobe shapes for a gauge length of 8 meters. If the gauge length increases, then lower wavenumbers can demonstrate these unusual behaviors for a fixed k, but as you continue to increase the gauge length, the sensitivity pattern fills in again (just as it would for very high k). However, seismic waves at these very high wavenumbers tend to die out quickly, so it is unlikely we could get much signal in these more filled in sensitivity trends seen for large k. But, we can force this fill-in by mimicking larger gauge lengths: averaging neighboring non-overlapping channels. This must be balanced with the loss in resolution. Further work is needed to develop a method to combine results from different apparent gauge lengths.

Consider that what may be an acceptable sensitivity pattern for type of wave may not be acceptable for another type. If we wish to force a sensitivity pattern more like a small kg, we should be able to decrease the apparent g in post-processing if (a) we record overlapping channels or (b) we record on a box that spits out two sets of data each corresponding to a different gauge length and those gauge lengths aren't multiples of each other. More details on the theory of why this should work can be found in the Appendix. Future work will include testing this theory.

CONCLUSIONS AND FUTURE WORK

In this report we derive the sensitivity patterns for horizontal DAS arrays reacting to various plane waves: P, S, Rayleigh and Love. Further, we compare the axial strain on orthogonal horizontal fibers to better understand trends, particularly polarity flips, observed at corners of existing DAS arrays. While point-wise axial strain starts to give us some insight into those trends, these results can mislead us with regards to the true data in two ways:

- The existence of frequency notches at certain frequencies and angles is not apparent in point strains,
- As wavenumber or gauge length increase, lobes in sensitivity may merge, expand or contract, but only when integrating over gauge lengths.

Thus, we also show sensitivity results for P, S, Rayleigh and Love waves detected through the average axial strain along a segment of fiber of length g. We extend these results to cross-correlation sensitivities of colinear channels detecting Rayleigh

waves and parallel channels detecting Love waves. Evidence suggests that for larger wavenumbers, the cross-correlation is primarily sensitive to waves traveling directly from one fiber to another. These results suggest there is some hope for ambient noise interferometry to yield reasonable results from DAS data.

However, there are some small details that we are continuing to investigate both theoretically and through the use of computational modeling:

- Parallel channels' lack of sensitivity to Love waves traveling directly through the radial direction between them could lead to small biases in velocities picked from cross-correlations. In the limit as kg grows, is ambient noise interferometry with an ideal noise field guaranteed to converge to Green's function extraction?
- For low wavenumbers in both the Love and Rayleigh wave interferometry cases, it is apparent that velocities picked from Love wave interferometry must be corrected for. What is a practical method to correct for this bias given limited knowledge of the subsurface velocity model?

ACKNOWLEDGEMENTS

E. Martin has also been supported in part by the DOE CSGF under grant number DE-FG02-97ER25308, and a Schlumberger Innovation Fellowship. We would like to thank OptaSense, particularly M. Karrenbach and S. Cole for the use of their ODH-3 interrogator unit and for many helpful suggestions as we worked with data from SDASA-1 to identify gaps in our understanding of sensitivity. We would also like to thank Jason Chang, Nori Nakata (University of Oklahoma), Nate Lindsey (University of California Berkeley), and Jonathan Ajo-Franklin (Lawrence Berkeley National Lab) for their insights and assistance.

REFERENCES

Biondi, B., E. Martin, S. Cole, and M. Karrenbach, 2017, Earthquakes analysis using data recorded by the stanford das array: SEP Report, **168**.

Bona, A., T. Dean, J. Correa, R. Pevzner, K. Tertyshnikov, and L. V. Zaanen, 2017, Amplitude and phase response of das receivers: 79th EAGE Conference & Exhibition Proceedings.

Kuvshinov, B., 2016, Interaction of helically wound fibre-optic cables with plane seismic waves: Geophysical Prospecting, **64**, 671–688.

Martin, E. and B. Biondi, 2017, Ambient noise interferometry across two-dimensional das arrays: Expanded Abstracts of the 87th Ann. Internat. Mtg.

Pujol, J., 2003, Elastic wave propagation and generation in seismology: Cambridge University Press.

APPENDIX: POINTWISE SENSITIVITY SHAPES ARE THE SAME AS ZERO WAVENUMBER SHAPE

For all wave types, the shape of the angular sensitivity could be considered to be the ratio between the geometric amplitude sensitvity term for any two angles, θ_1 and θ_2. The Rayleigh wave results were verified in this paper earlier. Here we verify this result for P-waves, Love waves, S-waves, which are nearly identical.

P-waves

Ratio between angles pointwise:

$$R(\theta_1, \theta_2) = \frac{\cos^2(\theta_1)\sin^2(\phi_1)}{\cos^2(\theta_2)\sin^2(\phi_2)} \tag{29}$$

The ratio between angles for a channel measurement:

$$R_c(\theta_1, \theta_2, k) = \frac{\cos(\theta_1)\sin(\phi_1)\sin(0.5kg\cos(\theta_1)\sin(\phi_1))}{\cos(\theta_2)\sin(\phi_2)\sin(0.5kg\cos(\theta_2)\sin(\phi_2))} \tag{30}$$

Take limit as $k \to 0$ with L'Hospital's rule:

$$\begin{aligned} R_c(\theta_1, \theta_2, 0) &= \frac{\cos(\theta_1)\sin(\phi_1)\cos(0.5 * 0 * g\cos(\theta_1)\sin(\phi_1))0.5g\cos(\theta_1)\sin(\phi_1)}{\cos(\theta_2)\sin(\phi_2)\cos(0.5 * 0 * g\cos(\theta_2)\sin(\phi_2))0.5g\cos(\theta_2)\sin(\phi_2)} \\ &= \frac{\cos^2(\theta_1)\sin^2(\phi_1)}{\cos^2(\theta_2)\sin^2(\phi_2)} \end{aligned} \tag{31}$$

Love waves

Ratio between angles pointwise:

$$R(\theta_1, \theta_2) = \frac{\cos(\theta_1)\sin(\theta_1)}{\cos(\theta_2)\sin(\theta_2)} \tag{32}$$

Ratio between angles for a full channel measurement:

$$R_c(\theta_1, \theta_2, k) = \frac{\sin(\theta_1)\sin(-0.5kg\cos(\theta_1))}{\sin(\theta_1)\sin(-0.5kg\cos(\theta_1))} \tag{33}$$

Take limit as $k \to 0$ and use L'Hospital's rule

$$\begin{aligned} R_c(\theta_1, \theta_2, 0) &= \frac{-0.5g\cos(\theta_1)\sin(\theta_1)\cos(-0.5 * 0 * g\cos(\theta_1))}{-0.5g\cos(\theta_2)\sin(\theta_2)\cos(-0.5 * 0 * g\cos(\theta_2))} \\ = \frac{\cos(\theta_1)\sin(\theta_1)}{\cos(\theta_2)\sin(\theta_2)} \end{aligned} \tag{34}$$

S-waves

Ratio between angles pointwise:

$$R(\theta_1, \theta_2) = \frac{\sin(\phi_1)\cos(\theta_1)(B\cos(\theta_1)\cos(\phi_1) + C\sin(\theta_1))}{\sin(\phi_2)\cos(\theta_2)(B\cos(\theta_2)\cos(\phi_2) + C\sin(\theta_2))} \tag{35}$$

Ratio between angles for a full channel measurement:

$$R_c(\theta_1, \theta_2, k) = \frac{(B\cos(\theta_1)\cos(\phi_1) + C\sin(\theta_1))\sin(-0.5kg\cos(\theta_1)\sin(\phi_1))}{(B\cos(\theta_2)\cos(\phi_2) + C\sin(\theta_2))\sin(-0.5kg\cos(\theta_2)\sin(\phi_2))} \tag{36}$$

Take limit as $k \to 0$ and use L'Hospital's rule:

$$\begin{aligned} R_c(\theta_1, \theta_2, k) &= \frac{-0.5g\cos(\theta_1)\sin(\phi_1)(B\cos(\theta_1)\cos(\phi_1) + C\sin(\theta_1))\cos(-0.5 * 0 * g\cos(\theta_1)\sin(\phi_1))}{-0.5g\cos(\theta_2)\sin(\phi_2)(B\cos(\theta_2)\cos(\phi_2) + C\sin(\theta_2))\cos(-0.5 * 0 * g\cos(\theta_2)\sin(\phi_2))} \\ &= \frac{\sin(\phi_1)\cos(\theta_1)(B\cos(\theta_1)\cos(\phi_1) + C\sin(\theta_1))}{\sin(\phi_2)\cos(\theta_2)(B\cos(\theta_2)\cos(\phi_2) + C\sin(\theta_2))} \end{aligned} \tag{37}$$

APPENDIX: RECOVERING SUB-GAUGE-LENGTH RESOLUTION FROM DAS

Say we have a DAS interrogator unit with channel spacing set at c meters, and gauge length g meters, and it's attached to a fiber of length nc meters. Then when the interrogator sends a laser pulse down the fiber, we observe $n-(g/c)+1$ measurements, $m_0, m_1, \ldots, m_{n-(g/c)}$, where

$$m_i = K\int_{ic}^{ic+g} s(x)dx \tag{38}$$

where s is the axial strain along the fiber parameterized by x, and K is some constant so m_i is a phase shift quasi-linearly proportional to s.

Frequently when geophysicists start using DAS, they have some confusion between gauge length and channel spacing, assuming that we always have $g = c$. This is often not the case, and in fact leads people to assume that their data have much smaller resolution than the raw data truly have. For instance, in SDASA-1, our active mode recording is $g = 7.14$, $c = 1.02$, so a new sensor of length 7.14 m begins every 1.02 m. Although we start a new measurement channel every 1.02 m, each measurement is the average axial strain over a 7.14 m segment.

Assuming that $g > c$ and that $g/c \in \mathbb{Z}_+$, we would like to reconstruct $\{u_i\}_{i=0}^{n-1}$ where

$$u_i = K\int_{ic}^{(i+1)c} s(x)dx \tag{39}$$

so one really can get the average strain for every meter along the fiber. We can express each measurement as a combination of the smaller scale measurements that could have been taken with a shorter gauge length as follows:

$$\begin{aligned} m_i &= K\int_{ic}^{ic+g} s(x)dx \\ &= K\left[\int_{ic}^{(i+1)c} s(x)dx + \int_{(i+1)c}^{(i+2)c} s(x)dx + \ldots + \int_{(i+(g/c)-1)c}^{(i+(g/c))c} s(x)dx\right] \\ &= u_i + u_{i+1} + \ldots + u_{i+(g/c)-1} \end{aligned} \tag{40}$$

This can be written as an underdetermined linear system where $\mathbf{u}$ is the unknown we wish to solve for:

$$\begin{bmatrix} m_0 \\ m_1 \\ \vdots \\ m_{n-(g/c)} \end{bmatrix} = \begin{bmatrix} 1 & \dots & 1 & 0 & \dots & & 0 \\ 0 & 1 & \dots & 1 & 0 & & 0 \\ \vdots & & \ddots & & \ddots & & \vdots \\ \vdots & & 0 & 1 & \dots & 1 & 0 \\ 0 & \dots & \dots & 0 & 1 & \dots & 1 \end{bmatrix} \begin{bmatrix} u_0 \\ u_1 \\ \vdots \\ u_{n-1} \end{bmatrix} \tag{41}$$

Let's call this matrix W, the weight matrix. For simplicity, we assume the integrals for averaging strain are uniformly weighted, so the bands of values in W are all 1's, but you could potentially imagine using other weightings. This is a $n - (g/c) + 1$ by n matrix, so $\mathbf{m} = W\mathbf{u}$ is an underdetermined system.

Possible solutions

We propose two potential fine-scale measurement recovery methods:

- Keep the underdetermined system, perform a regularized inversion, and play around with starting points or random noise to see how sensitive your system is to its null-space.
- Add enough independent rows to W so it will be invertible, or even add enough rows that it becomes an overdetermined system. This can be done by making simultaneous measurements with a gauge length g' that's not a factor or multiple of g.

Regularized inversion

How it works: Find the u that minimizes the misfit, while not blowing up:

$$\min_{u \in \mathbb{R}^n} \|Wu - m\|_2^2 + \lambda \|u\|_2^2 \tag{42}$$

although $\|u\|_2^2$ could be replaced with some other regularization.

Pros: Does not require any modifications to acquisition. Can be tested using the 1 meter spaced nodes from the active survey in March 2017 on Stanford campus.

Cons: Not guaranteed to return v_i for any i. Likely to smooth out measurements (depending on regularization type). It is not totally obvious how to choose λ.

Multiple simultaneous gauge lengths

How it works: At (roughly) the same time that the first gauge length's measurements are taken, also measure $\{m'_i\}_{i=0}^{n-(g'/c)}$, defined in the same way but for gauge length $g' > c$, where g' is neither a multiple or a diviser of g. Then new rows are added to the weight matrix representing the equations:

$$m'_i = u_i + u_{i+1} + \ldots + u_{i+(g'/c)-1} \tag{43}$$

so the new matrix, W' has the same structure as W except g'/c bands instead of g/c bands, and it contains $n - (g'/c) + 1$ rows. Thus the system

$$\begin{bmatrix} \mathbf{m} \\ \mathbf{m}' \end{bmatrix} = \begin{bmatrix} W \\ W' \end{bmatrix} \mathbf{u} \tag{44}$$

which is an overdetermined system that can be solved via least-squares. Since this system must be solved at each time step for u, it makes sense to directly invert the sparse matrix $W^T W + W'^T W'$, then the solution can be done via a matrix multiplication. This can be done for more than two gauge lengths also, but two should be sufficient.

Note: if g' is a multiple or divisor of g, the system is still rank deficient. If g and g' are close (say 9 and 10 m) the condition number is lower (around a few hundred, relatively independent of n) and the system tends to behave better.

Pros: Guaranteed to return $\{u_i\}_{i=0}^{n-1}$ up to noise levels. Different gauge lengths (that aren't multiples of each other) also means reduced effect from frequency notches. Even with just two gauge lengths, the system is already overdetermined which helps with robustness in the face of noise.

Cons: Requires a different interrogator unit configuration than is available.